



**HAL**  
open science

## Dynamic imaging reveals surface exposure of virulent *Leishmania amastigotes* during pyroptosis of infected macrophages

Thibault Rosazza, Hervé Lecoœur, Thierry Blisnick, Maryse Moya-Nilges, Pascale Pescher, Phillipe Bastin, Eric Prina, Gerald Späth

► **To cite this version:**

Thibault Rosazza, Hervé Lecoœur, Thierry Blisnick, Maryse Moya-Nilges, Pascale Pescher, et al.. Dynamic imaging reveals surface exposure of virulent *Leishmania amastigotes* during pyroptosis of infected macrophages. *Journal of Cell Science*, 2020, pp.jcs.242776. 10.1242/jcs.242776 . pasteur-02779320

**HAL Id: pasteur-02779320**

**<https://pasteur.hal.science/pasteur-02779320>**

Submitted on 4 Jun 2020

**HAL** is a multi-disciplinary open access archive for the deposit and dissemination of scientific research documents, whether they are published or not. The documents may come from teaching and research institutions in France or abroad, or from public or private research centers.

L'archive ouverte pluridisciplinaire **HAL**, est destinée au dépôt et à la diffusion de documents scientifiques de niveau recherche, publiés ou non, émanant des établissements d'enseignement et de recherche français ou étrangers, des laboratoires publics ou privés.



Distributed under a Creative Commons Attribution - NonCommercial - ShareAlike 4.0 International License

# **DYNAMIC IMAGING REVEALS SURFACE EXPOSURE OF VIRULENT *LEISHMANIA* AMASTIGOTES DURING PYROPTOSIS OF INFECTED MACROPHAGES**

Thibault Rosazza<sup>1\*</sup>, Hervé Lecoœur<sup>1,2\*</sup>, Thierry Blisnick<sup>3</sup>, Maryse Moya-Nilges<sup>4</sup>, Pascale Pescher<sup>1</sup>, Phillipe Bastin<sup>3</sup>, Eric Prina<sup>1</sup> and Gerald F. Späth<sup>1,2</sup>.

<sup>1</sup>Institut Pasteur, Unité de Parasitologie Moléculaire et Signalisation, INSERM U1201, Paris, France

<sup>2</sup>Institut Pasteur International Mixed Unit 'Inflammation and *Leishmania* infection',

<sup>3</sup>Institut Pasteur, Trypanosome Cell Biology Unit & INSERM U1201, Paris, France

<sup>4</sup>Institut Pasteur, Unité de Technologie et service BioImagerie Ultrastructurale (UtechSPBI),

\*co first authors

thibault.rosazza@gmail.com, 2392267@dundee.ac.uk

herve.lecoeur@pasteur.fr

eric.prina@pasteur.fr

gerald.spaeth@pasteur.fr

maryse.moya-nilges@pasteur.fr

thierry.blisnick@pasteur.fr

philippe.bastin@pasteur.fr

pascale.pescher@pasteur.fr

## **Keywords**

*Leishmania*, macrophage, pyroptosis, high-content, single-cell, real-time imaging, virulence

## Abstract

*Leishmania* spp are obligate intracellular parasites that infect phagocytes, notably macrophages. No information is available on how *Leishmania* parasites respond to pyroptosis of their host cell, known to limit microbial infection. Here, we analyzed the pyroptotic process and the fate of intracellular amastigotes at the single cell level using high-content, real-time imaging. Bone marrow-derived macrophages were infected with virulent *L. amazonensis* amastigotes and sequentially treated with lipopolysaccharide and adenosine triphosphate for pyroptosis induction. Real-time monitoring identified distinct pyroptotic phases, including rapid decay of the parasitophorous vacuole (PV), progressive cell death, and translocation of the luminal PV membrane to the cell surface in 40% of macrophages, resulting in the extracellular exposure of amastigotes that remained anchored to PV membranes. Electron microscopy analyses revealed an exclusive polarized orientation of parasites, with the anterior pole exposed toward the extracellular milieu, and the parasite posterior pole attached to the PV membrane. Exposed parasites retain their full infectivity towards naïve macrophages suggesting that host cell pyroptosis may contribute to parasite dissemination.

## Introduction

*L. amazonensis* is one of the etiologic agents of human, localized cutaneous and anergic diffuse cutaneous leishmaniasis in South America (Barral et al., 1991; Silveira et al., 2004). Restriction of intracellular *L. amazonensis* replication *in vitro* and *in vivo* was shown to depend on the NLRP3 (NOD-, LRR- and pyrin domain-containing protein 3) inflammasome (Zamboni and Sacks, 2019). This intracellular sensor is induced in response to a “priming signal” represented by cytokines or ligands of Toll-like receptors, and further activated by damage-associated molecular patterns (DAMPs), such as adenosine triphosphate (ATP). Inflammasome activation triggers caspase-1 activity, which cleaves pro-IL-1 $\beta$  and pro-IL-18 into mature cytokines - promoting an anti-microbial, pro-inflammatory immune response (Swanson et al., 2019) - and cleaves gasdermin D that forms pores inside the macrophage plasma membrane, sustaining IL-1 $\beta$  release (Lieberman et al., 2019) and causing pyroptosis (Bergsbaken et al., 2009; Fink and Cookson, 2006; Jorgensen et al., 2017; Shi et al., 2015). Significantly, pyroptotic cell death contributes to a protective response against intracellular pathogens by removing the niche for infection (Bergsbaken et al., 2009), by exposing microbes to the immune system (Jorgensen and Miao, 2015), and by rendering pathogens more susceptible to anti-microbial agents (Jorgensen et al., 2016) or direct microbial killing (Liu et al., 2016).

Even though the interaction of *L. amazonensis* with the NLRP3 inflammasome has attracted considerable attention (Lecoeur et al., 2020; Lima-Junior et al., 2013), how pyroptosis affects parasite survival and virulence remains to be elucidated. Here, we deployed a real-time, high-content single-cell analysis that uncovers unique features of *Leishmania* amastigotes during host macrophage pyroptosis.

## Materials & Methods

### Ethics statement

Animals were housed at the Institut Pasteur animal facilities accredited by the French Ministry of Agriculture for performing experiments on live rodents. Work on animals was performed in compliance with French and European regulations on care and protection of laboratory animals (EC Directive 2010/63, French Law 2013-118, February 6th, 2013). All experiments were approved by the Ethic Committee for animal experimentation (CETEA#89) and authorized by the French ministry of higher education, research and innovation under the reference 2013-0092 in accordance with the Ethics Charter of animal experimentation that includes respect of the 3Rs principles, appropriate procedures to minimize pain and animal suffering.

### Bone Marrow-Derived Macrophage cultures

Female C57BL/6 mice were obtained from Janvier (Saint Germain-sur-l'Arbresle, France). Bone marrow cell suspensions were recovered from tibias and femurs as described (Courret et al., 1999). Bone marrow cells were plated at  $1.5 \times 10^7$  cells/mL in hydrophobic Petri dishes (# 664161, Corning Life Science) and cultured for 6 days at 37°C in a 7.5% CO<sub>2</sub> air atmosphere in complete DMEM medium (# P04-03500, Pan Biotech) containing 4.5 g/L Glucose, 2 mM L-Glutamine, 1 mM sodium pyruvate and 3.7 g/L NaHCO<sub>3</sub> and supplemented with 15% FCS (# A3160801, Gibco), 10 mM HEPES (# 15630080, Gibco), 50 µg/mL Penicillin/Streptomycin (# P4333, Sigma-Aldrich), 50 µM 2-Mercaptoethanol (# M6250, Sigma-Aldrich) and with 75 ng/mL recombinant mouse CSF-1 (#234311, ImmunoTools). Adherent bone marrow-derived macrophages (BMDMs) were recovered and seeded in complete DMEM medium supplemented with 30 ng/mL rmCSF-1 into various culture-treated supports, including (i) flat bottom 96-well black µClear® plates (# 655090, Greiner Bio-One) for OPERA analyses, (ii) 24-well plates (# 353047, Corning, Falcon®) with glass coverslips inside for scanning electron microscopy analyses, and (iii) 6-well plates (# 353046, Dutscher, Falcon®) for amastigote isolation from infected BMDMs.

### Macrophage infection and activation

*Leishmania amazonensis* amastigotes (LV79 strain, MPRO/BR/72/M1841) expressing mCherry (Lecoeur et al., 2020) were isolated from footpad lesions of infected Swiss nu/nu mice

and purified as described (Courret et al., 1999). Infections were carried out at 34°C at a ratio of four amastigotes per macrophage. *Leishmania donovani* amastigotes (Ld1S2D strain, MHOM/SD/62/1S-CL2D) were isolated from infected spleens of female RjHan:AURA Golden Syrian hamsters and purified as described (Pescher et al., 2011; Prieto Barja et al., 2017). Infections were carried out at 37°C at a ratio of eight amastigotes per macrophage.

All pyroptosis experiments were performed after 3 days of infection using a sequential treatment of 500 ng/ml lipopolysaccharide (# LPS11-1, Alpha Diagnostic) for 4 hours and 5 mM ATP (# A26209, Sigma-Aldrich) for different periods up to 4 hours.

### **Real time analysis of pyroptosis by confocal microscopy**

The following fluorescent reporters were added to the cell cultures 15 min before ATP stimulation: Hoechst 33342 (10 µg/mL) (# H3570, Invitrogen), LysoTracker Green DND-26 (1 µM) (LTG, # L7526, Invitrogen), YO-PRO-1 (1 µM) (# Y3603, Invitrogen). The pyroptotic process was monitored at 34°C and 7.5% CO<sub>2</sub> using a fully automated spinning disk confocal microscope OPERA™ quadruple Excitation High Sensitivity (QEHS, PerkinElmer Technologies) with a 40x water immersion objective (Aulner et al., 2013). Image acquisition was performed every five minutes after ATP addition using the following sequential acquisition settings: (i) 405 nm laser line excitation, filter 450/50 for Hoechst 33342 detection, (ii) 488 nm laser line excitation, filter 540/75 for LTG or YO-PRO-1 detection and (iii) 561 nm laser line excitation, filter 600/40 for mCherry detection. Additionally, transmission light microscopy images were taken for analyses of the macrophage PV area and amastigote localization. Fifteen fields at the same focal plane were taken every 5 minutes for every channel and for each sample. Images were transferred to the Columbus Conductor™ Database (Perkin Elmer Technologies) for storage and further analysis using specific scripts (Fig. S1). Single-cell analyses were performed using the ImageJ software package (<https://imagej.nih.gov/ij/docs/faqs.html>).

### **Scanning and transmission electron microscopy analyses**

Pyroptotic BMDMs were fixed overnight with 2.5% glutaraldehyde in 0.1 M cacodylate buffer (pH 7.2) at 4°C and post-fixed in 0.1 M cacodylate buffer (pH 7.2) containing 1% OsO<sub>4</sub>. After serial dehydration, samples were critical-point dried (Emitech K850 or Balzers Union CPD30) and coated with gold using a sputter coater (Gatan Ion Beam Coater 681). Scanning electron

microscopy observations were made with the JEOL 7600F microscope. Images were colorized using Adobe Photoshop CS software.

For transmitted electron microscopy analysis, cells were cultured on coverslips and were fixed with 2.5% of glutaraldehyde (Sigma-Aldrich) in PHEM buffer (120 mM PIPES, 50 mM HEPES, 20 mM EGTA, 4 mM MgCl<sub>2</sub>, pH 7.3). Post fixation was done with 1% osmium tetroxide (EMS 19152 2% aqueous solution, Merck) and 1.5% ferrocyanide (# 8131, Sigma-Aldrich) in PHEM. After dehydration by a graded series of ethanol from 25 to 95% grade 1 (99.8% pure ethanol), the samples were infiltrated with epoxy resin. The 70 nm sections obtained by thin sectioning using a Leica UC 7 microtome (Leica Microsystems), were collected on formvar coated slot grids (EMS 215-412-8400) and were contrasted with 4% uranyl acetate and Reynolds lead citrate (#11300, Delta Microscopies,). Stained sections were observed with a Tecnai spirit FEI operated at 120 kV. Images were acquired with FEI Eagle digital camera.

### **Western blotting**

Cells were lysed in RIPA buffer (# R0278, Sigma-Aldrich) supplemented with a cocktail of anti-proteases and anti-phosphatases inhibitors (MS-SAFE, Sigma-Aldrich). Proteins were resolved by SDS-PAGE on NuPAGE gels (4–12% Bis-Tris) in MOPS buffer and electroblotted onto polyvinylidene difluoride (PVDF) membranes in transfer buffer (Lecoeur et al., 2020). Membranes were blocked with 5% fat-free milk in 1×Tris-buffered saline containing 0.25% Tween 20 and then probed overnight at 4°C with anti-capase-1 antibody (# AG-20B-0042, Adipogen Life Sciences) and further incubated with anti-mouse peroxydase conjugate secondary antibodies. Membranes were revealed by SuperSignal West Pico reagent (#10481945, Thermo Fisher Scientific) in a high-resolution PXi machine (Syngene).

### **Amastigote isolation from pyroptotic and control macrophages**

Supernatants of BMDM cultures (pyroptotic and control BMDMs) were carefully replaced by fresh medium without LPS/ATP. After detaching adherent macrophages using a plastic cell scraper (# 541070, Greiner bio-one) and multiple passages through a 27-gauge needle to free amastigotes from cell remnants, isolated amastigotes were centrifuged, washed in PBS, counted and used to assess parasite viability, the capacity of amastigotes to differentiate into proliferating promastigotes *in vitro*, and amastigote virulence by infection of naïve BMDMs.

### **Flow cytometric analysis of parasite death by YO-PRO-1 staining**

Amastigotes isolated from *Leishmania*-infected, pyroptotic and control BMDMs were seeded in a 96-well plate (# 353072, Dutcher, Falcon®) at a final concentration of  $5 \times 10^6$  parasites per mL and incubated for 10 min with YO-PRO-1™ iodide at 0.1  $\mu$ M final concentration (# Y3603, Thermo Fisher Scientific). Samples were then immediately analyzed on the CytoFLEX cytometer (Beckman Coulter) in a BSL2 containment to evaluate YO-PRO-1 incorporation. Data were analyzed using the Kaluza 1.5 software (Beckman Coulter Life Sciences). Lesion-derived amastigotes were treated with 70% Ethanol for 10 min and were included as positive control for cell death and YO-PRO-1 incorporation.

### **Analysis of parasite differentiation, growth and metabolic status**

Amastigote to promastigote differentiation was analyzed by scanning electron microscopy (as described above) directly on amastigotes exposed on pyroptotic macrophages after 24 hours incubation in 1 mL of promastigote culture medium at 27°C. For growth analysis in culture, purified amastigotes were incubated at 27°C in promastigote culture medium at  $10^5$  parasites / mL. Promastigote culture density was determined daily during 6 consecutive days by visual counting using a Malassez chamber. The parasite metabolic status was analyzed at days 2 and 3 by resazurin assay. Briefly, 200  $\mu$ l of parasite culture was transferred into wells of a 96-well plate (# 655090, Sigma-Aldrich) and incubated with 2.5  $\mu$ g/mL of resazurin (# R7017, Sigma-Aldrich) for 4 hours at 27°C. The fluorescence intensity of the resazurin-derived resorufin was determined using the Tecan Safire2 plate reader (558 nm excitation, 585 nm emission) (Lamotte et al., 2019).

### **Determination of amastigote virulence**

Amastigote virulence was assessed using two protocols. First, isolated amastigotes from *Leishmania*-infected, pyroptotic and control BMDMs were added at a ratio of four parasite per macrophages on naive BMDMs seeded on glass coverslips placed in 24-well plates. One and two days after incubation at 34°C, amastigote-infected BMDMs were fixed with 4% paraformaldehyde (PFA) (# 15710, Electron Microscopy Sciences) and incubated for 10 min in PBS containing 10  $\mu$ g/mL of Hoechst 33342. Image acquisition was performed with the Axio Imager (Zeiss) (405 nm laser line excitation, filter 450/50). The number of parasites per



macrophage was determined by visual counting, considering at least one hundred macrophages. Second, the culture medium of pyroptotic macrophages was carefully replaced by pre-warmed BMDM medium containing freshly differentiated, naïve BMDMs (1:1 ratio between naïve and pyroptotic BMDMs). Three days later, live-images combining bright field and mCherry fluorescence were acquired using the EVOS microscope (Thermo Fisher Scientific) and analyzed with the FIJI software for infection of the naïve BMDMs.

## RESULTS AND DISCUSSION

### **A high-content imaging protocol for dynamic single-cell analysis of pyroptotic macrophages infected by *L. amazonensis* amastigotes**

To analyze the dynamics of pyroptosis in *L. amazonensis*-infected macrophages, we established a new imaging protocol combining high-content and single-cell analyses using the OPERA™ QEHS confocal plate reader (Fig. 1A). Bone marrow-derived macrophages (BMDMs) were seeded into 96 well plates (macrophage settlement). They were subsequently infected for three days with mCherry transgenic, virulent amastigotes isolated from lesions of infected Nude mice, allowing to form characteristic communal PVs (parasite settlement). Then, LPS was added for 225 min (NLRP3 priming) followed by staining with fluorescent reporters. Pyroptosis was triggered after NLRP3 activation by ATP (pyroptosis induction). Dynamic cellular changes were monitored at high-content and single-cell levels by using Hoechst 33342 (for cell number, Fig. 1B1), YO-PRO-1 (for loss of plasma membrane (PM) integrity, Fig. 1B2) (Adamczak et al., 2014), LysoTracker green (LTG, for PV acidity, Fig. 1B3) (Aulner et al., 2013), and mCherry (for parasite localization, Fig. 1B4) (Aulner et al., 2013). Macrophage morphology was analyzed by transmission light microscopy (TL, Fig. 1B5). High-Content Assay (HCA) analyses were carried out in real-time up to 240 min post ATP addition. Analyses at the population level were performed using segmentation procedures (Fig. S1A, B). The analysis of fluorescent read-outs at 240 min documented that (i) no macrophages were lost during the analyses (Fig. 1C1), (ii) pyroptosis induction was successful (Fig. 1C2), and the PV integrity was lost in all pyroptotic cells (Fig. 1C3). The induction of pyroptosis by LPS/ATP in *L. amazonensis*-infected macrophages was validated by monitoring cell morphology (Fig. S2A), caspase-1 cleavage and release (Fig. S2B) and IL-1 $\beta$  secretion (Fig. S2C). Single-cell analyses permitted to determine macrophage / PV area and parasite location (Fig. 1D).

## **Rapid decay of PV precedes amastigote extracellular exposure during macrophage pyroptosis**

Pyroptosis dynamics, PV integrity and parasite localization were analyzed every 5 min after ATP addition for a duration of 240 min in infected, LPS-primed macrophages. HCA analysis of YO-PRO-1 incorporation revealed that pyroptosis was asynchronous as judged by the progressive increase in dead cells (Fig. 2A, black curve). Pyroptosis occurred with a constant rate ( $+18.2 \pm 4.2\%$  of cell death per hour). A loss of LTG staining revealed that PVs rapidly decayed (Fig. 2A, green curve), following three distinct empirical rates: (i) a fast decay rate during the first 45 minutes ( $-4.2 \times 10^6 \pm 1.2 \times 10^6 / 30$  min, stage 1) leading to a 47.6% decrease of LTG fluorescence intensity, (ii) an intermediate rate (45 to 120 min,  $-1.2 \times 10^6 \pm 6.3 \times 10^5 / 30$  min, stage 2), and (iii) a slow rate thereafter ( $0.58 \times 10^6 \pm 0.37 \times 10^6 / 30$  min, stage 3). This decay may result from ATP-induced changes of the vacuolar pH and of PV integrity that could be caused by osmotic changes similar to those described for lysosomes (Guha et al., 2013; Takenouchi et al., 2009). Single-cell analyses revealed differences in the PV decay kinetics between macrophages (Fig. S3A-D) as well as between PVs inside a same macrophage (Fig. 2B1 - 3). Monitoring individual PVs revealed progressive reduction of PV area and loss of about half of the PVs at the final time point (T) 240 min (Fig. S3B). Interestingly, the decrease of PV area is more pronounced in large PVs (area superior to 2000 square pixels) than in smaller ones (area inferior to 1000 square pixels) (Fig. S3C).

HCA analysis revealed that amastigotes either remained intra-vacuolar (62% of macrophages) or were exposed at the cell surface (38% of macrophages) as shown in representative cells (Fig. 2B1 and 2B2, Fig. S3A). Significantly, different decay rates and parasite localizations were observed for individual PVs, even inside the same macrophage as indicated in Fig. 2B2, showing three independent vacuoles (a, b and c) that rapidly lost LTG fluorescence (stage 1). PVs (a) and (b) displayed a moderate decrease in size and retained intracellular amastigotes (Fig. 2B2 and 2B3), whereas PV (c) collapsed (60 min) and the luminal side of its membrane was exposed to the extracellular milieu (120 min, stage 2). PV lumen exposure could be triggered by ATP as judged by previous reports implicating ATP in the extracellular discharge of secretory exosomes (Andrei et al., 2004; Bergsbaken et al., 2011), in exosome exocytosis (Qu et al., 2007), or in the release of auto-phagolysosomes and phagocytosed, intracellular particles (Bergsbaken et al., 2011; Takenouchi et al., 2009). Amastigote exposure occurred preferentially in macrophages displaying a rapid PV decay (Fig.

2, Fig. S3). Additionally, parasite exposure neither correlates with PV size, PV number nor amastigote number per vacuole (data not shown). In contrast, PVs that display a high area value and that rapidly expose parasites - such as PV (c) (Fig. 2B2) - decayed faster than other PVs (Fig. S3C-D).

### **Ultrastructural analysis of amastigote attachment zone and surface exposure**

Pyroptosis has been recognized as an anti-microbial strategy during bacterial infection, capable of pathogen trapping inside dying host cells (Jorgensen et al., 2016) and directly killing bacteria (Liu et al., 2016). Our observation that amastigotes remain attached on the surface of pyroptotic cells primed us to investigate parasite integrity and the molecular structures underlying parasite surface retention.

Scanning electron microscopy analyses showed that 38.8% of pyroptotic macrophages displayed intact parasites at the cell surface (Figs. 3A1, 3A2, and Fig. S3E, F), thus confirming our results obtained with the OPERA™ system (Fig. 2). Ultrastructural analysis demonstrated that exposed amastigotes remained attached at macrophage membranes. Significantly, exposed amastigotes showed a highly polarized orientation with only the anterior pole (flagellar side) being exposed toward the extracellular milieu. This feature was also observed for pyroptotic macrophages infected with *L. donovani* amastigotes that reside in individual PVs (Fig. S3G). We next investigated the posterior attachment zone by Transmission Electron Microscopy (TEM), which revealed an electro-dense, membranous junction formed between parasite and PV membranes both in non-stimulated and pyroptotic macrophages (Figs. 3B1, 3B2). This junction corresponds to a defined attachment site - showing features similar to gap junctions - that permits amastigotes of communal *Leishmania* species to be anchored to PV membranes (Benchimol and de Souza, 1981). These results demonstrate that amastigotes remain strongly attached to pyroptotic macrophages through their attachment site (see supplementary data, Movie 1), which represents a new type of interaction observed in pyroptotic cells, different from the one previously described in the literature (Jorgensen et al., 2016).

## ***Leishmania amazonensis* amastigotes are resistant to host cell pyroptosis and retain full infectivity**

Since bacteria can be damaged during host cell pyroptosis (Liu et al., 2016), we next investigated whether parasite viability and infectivity were affected during macrophage pyroptosis. Amastigotes isolated from pyroptotic macrophages (A-pm) were compared to amastigotes isolated from unstimulated control macrophages (A-cm). Macrophage pyroptosis did not reduced parasite viability (99% of A-pm remained YO-PRO-1 negative, Fig. 4A1). Second, when pyroptotic macrophages were cultured in promastigote-specific medium (48 hours, 27°C), amastigotes rapidly transformed into ovoid flagellated, motile and proliferating promastigotes that detached from macrophage remnants (Fig. 4A2). These promastigotes showed normal growth (visual parasite counting, Fig. 4A3) and metabolic activity (resazurin reduction data, Fig. 4A4). Finally, A-pm maintained their capacity to establish efficient new infections (Fig. 4B). In addition, amastigotes associated to macrophage remnants were efficiently phagocytosed by naïve BMDMs and established normal infection levels as shown by the formation of typical large communal PVs housing numerous parasites after 3-day co-culture (Fig. 4C3).

## **CONCLUSION**

We analyzed dynamic interactions between *Leishmania* amastigotes and PVs in pyroptotic BMDMs at the population, single-cell and ultrastructural levels. Real-time HCA analysis uncovered three distinct stages of the pyroptotic process in our experimental system (Fig. S4): During stage 1, the PV membrane decays (rapid loss of PV acidity and reduced PV size). In stage 2, the PV lumen is externalized in 38% of cells, resulting in exposure of membrane-anchored amastigotes. In stage 3, cellular alterations are further sustained (80% of cell death). *L. amazonensis* amastigotes retained their viability and infectivity during macrophage pyroptosis. We therefore can speculate that parasites attached to pyroptotic cell debris *in vivo* may favor parasite spreading - as shown for other forms of host cell death – allowing for uptake by macrophages newly recruited to inflammatory infection sites (de Menezes et al., 2016). On the other hand, the extracellular exposure of amastigotes could expose parasites to complement-dependent cytotoxicity that is known to control parasite load *in vivo* (Laurenti et al., 2004), or to anti-leishmanial antibodies that could promote cell-mediated cytotoxicity via Fc receptor-

dependent phagocytosis. Our results will stimulate future studies designed to assess the role of macrophage pyroptosis in *Leishmania* dissemination, transmission, and immuno-pathology.

### **Acknowledgements**

We thank Drs Jacomina Krijnse Locker and Geneviève Milon for scientific discussions, and Dr Nathalie Aulner for help with the Opera system.

### **Funding**

This project was supported by i) a fund of the Institut Pasteur International Direction (International Mixed Unit ‘Inflammation and Leishmania infection’), ii) the French National Research Agency (ANR-10-INSB-04-01, Investments for the Future), the Conseil de la Region Ile-de-France (program Sesame 2007, project Imagopole, S. Shorte) and the Fondation Française pour la Recherche Médicale (Programme Grands Equipements) (UtechS PBI/C2RT), iii) a French Government Investissement d’Avenir programme, Laboratoire d’Excellence “Integrative Biology of Emerging Infectious Diseases” (ANR-10-LABX-62-IBEID) (Trypanosome Cell Biology and Molecular Parasitology and Signaling Units), and iv) a fund from Institut Pasteur (PTR 496).

### **Competing interests**

Authors have no competing interest.

### **Author contributions**

TR, MMN, TB and PP performed experiments and analyzed the data. TR, HL and EP designed the experiments, and analyzed the data. HL, EP and GFS wrote the manuscript. PB planned EM analyses, scientific discussions, and correction of the manuscript.

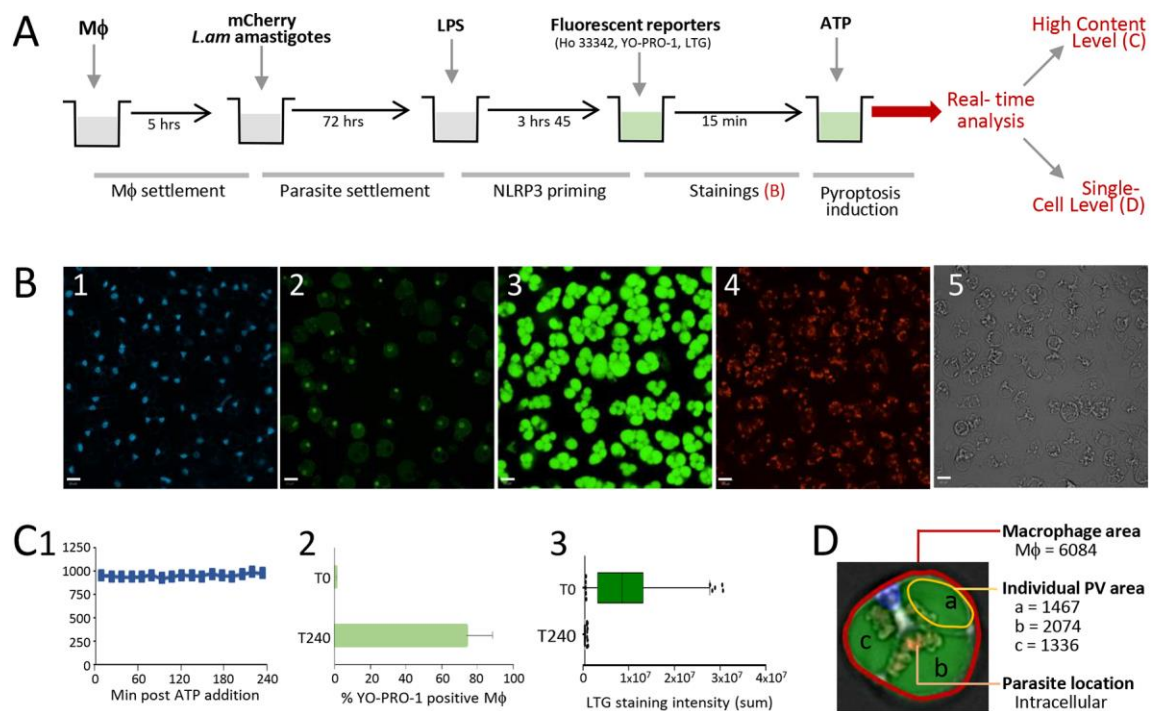
## Bibliography

- Adamczak, S.E., de Rivero Vaccari, J.P., Dale, G., Brand, F.J., 3rd, Nonner, D., Bullock, M.R., Dahl, G.P., Dietrich, W.D., and Keane, R.W.** (2014). Pyroptotic neuronal cell death mediated by the AIM2 inflammasome. *Journal of cerebral blood flow and metabolism : official journal of the International Society of Cerebral Blood Flow and Metabolism* **34**, 621-629.
- Andrei, C., Margiocco, P., Poggi, A., Lotti, L.V., Torrisi, M.R., and Rubartelli, A.** (2004). Phospholipases C and A2 control lysosome-mediated IL-1 beta secretion: Implications for inflammatory processes. *Proceedings of the National Academy of Sciences of the United States of America* **101**, 9745-9750.
- Aulner, N., Danckaert, A., Rouault-Hardoin, E., Desrivot, J., Helynck, O., Commere, P.H., Munier-Lehmann, H., Spath, G.F., Shorte, S.L., Milon, G., et al.** (2013). High content analysis of primary macrophages hosting proliferating *Leishmania* amastigotes: application to anti-leishmanial drug discovery. *PLoS neglected tropical diseases* **7**, e2154.
- Barral, A., Pedral-Sampaio, D., Grimaldi Junior, G., Momen, H., McMahon-Pratt, D., Ribeiro de Jesus, A., Almeida, R., Badaro, R., Barral-Netto, M., Carvalho, E.M., et al.** (1991). Leishmaniasis in Bahia, Brazil: evidence that *Leishmania amazonensis* produces a wide spectrum of clinical disease. *The American journal of tropical medicine and hygiene* **44**, 536-546.
- Benchimol, M., and de Souza, W.** (1981). *Leishmania mexicana amazonensis*: attachment to the membrane of the phagocytic vacuole of macrophages in vivo. *Zeitschrift fur Parasitenkunde* **66**, 25-29.
- Bergsbaken, T., Fink, S.L., and Cookson, B.T.** (2009). Pyroptosis: host cell death and inflammation. *Nature reviews Microbiology* **7**, 99-109.
- Bergsbaken, T., Fink, S.L., den Hartigh, A.B., Loomis, W.P., and Cookson, B.T.** (2011). Coordinated host responses during pyroptosis: caspase-1-dependent lysosome exocytosis and inflammatory cytokine maturation. *Journal of immunology* **187**, 2748-2754.
- Courret, N., Prina, E., Mougneau, E., Saraiva, E.M., Sacks, D.L., Glaichenhaus, N., and Antoine, J.C.** (1999). Presentation of the *Leishmania* antigen LACK by infected macrophages is dependent upon the virulence of the phagocytosed parasites. *European journal of immunology* **29**, 762-773.
- de Menezes, J.P., Saraiva, E.M., and da Rocha-Azevedo, B.** (2016). The site of the bite: *Leishmania* interaction with macrophages, neutrophils and the extracellular matrix in the dermis. *Parasites & vectors* **9**, 264.
- Fink, S.L., and Cookson, B.T.** (2006). Caspase-1-dependent pore formation during pyroptosis leads to osmotic lysis of infected host macrophages. *Cellular microbiology* **8**, 1812-1825.
- Guha, S., Baltazar, G.C., Coffey, E.E., Tu, L.A., Lim, J.C., Beckel, J.M., Patel, S., Eysteinson, T., Lu, W., O'Brien-Jenkins, A., et al.** (2013). Lysosomal alkalization, lipid oxidation, and reduced phagosome clearance triggered by activation of the P2X7 receptor. *FASEB journal : official publication of the Federation of American Societies for Experimental Biology* **27**, 4500-4509.
- Jorgensen, I., and Miao, E.A.** (2015). Pyroptotic cell death defends against intracellular pathogens. *Immunological reviews* **265**, 130-142.
- Jorgensen, I., Rayamajhi, M., and Miao, E.A.** (2017). Programmed cell death as a defence against infection. *Nature reviews Immunology* **17**, 151-164.
- Jorgensen, I., Zhang, Y., Krantz, B.A., and Miao, E.A.** (2016). Pyroptosis triggers pore-induced intracellular traps (PITs) that capture bacteria and lead to their clearance by efferocytosis. *The Journal of experimental medicine* **213**, 2113-2128.
- Lamotte, S., Aulner, N., Spath, G.F., and Prina, E.** (2019). Discovery of novel hit compounds with broad activity against visceral and cutaneous *Leishmania* species by comparative phenotypic screening. *Scientific reports* **9**, 438.
- Laurenti, M.D., Orn, A., Sinhorini, I.L., and Corbett, C.E.** (2004). The role of complement in the early phase of *Leishmania (Leishmania) amazonensis* infection in BALB/c mice. *Brazilian journal of medical and biological research = Revista brasileira de pesquisas medicas e biologicas* **37**, 427-434.

- Lecoeur, H., Prina, E., Rosazza, T., Kokou, K., N'Diaye, P., Aulner, N., Varet, H., Bussotti, G., Xing, Y., Milon, G., et al.** (2020). Targeting Macrophage Histone H3 Modification as a *Leishmania* Strategy to Dampen the NF-kappaB/NLRP3-Mediated Inflammatory Response. *Cell Rep* **30**, 1870-1882 e1874.
- Lieberman, J., Wu, H., and Kagan, J.C.** (2019). Gasdermin D activity in inflammation and host defense. *Science immunology* **4**.
- Lima-Junior, D.S., Costa, D.L., Carregaro, V., Cunha, L.D., Silva, A.L., Mineo, T.W., Gutierrez, F.R., Bellio, M., Bortoluci, K.R., Flavell, R.A., et al.** (2013). Inflammasome-derived IL-1beta production induces nitric oxide-mediated resistance to *Leishmania*. *Nature medicine* **19**, 909-915.
- Liu, X., Zhang, Z., Ruan, J., Pan, Y., Magupalli, V.G., Wu, H., and Lieberman, J.** (2016). Inflammasome-activated gasdermin D causes pyroptosis by forming membrane pores. *Nature* **535**, 153-158.
- Pescher, P., Blisnick, T., Bastin, P., and Spath, G.F.** (2011). Quantitative proteome profiling informs on phenotypic traits that adapt *Leishmania donovani* for axenic and intracellular proliferation. *Cellular microbiology* **13**, 978-991.
- Prieto Barja, P., Pescher, P., Bussotti, G., Dumetz, F., Imamura, H., Kedra, D., Domagalska, M., Chaumeau, V., Himmelbauer, H., Pages, M., et al.** (2017). Haplotype selection as an adaptive mechanism in the protozoan pathogen *Leishmania donovani*. *Nature ecology & evolution* **1**, 1961-1969.
- Qu, Y., Franchi, L., Nunez, G., and Dubyak, G.R.** (2007). Nonclassical IL-1 beta secretion stimulated by P2X7 receptors is dependent on inflammasome activation and correlated with exosome release in murine macrophages. *Journal of immunology* **179**, 1913-1925.
- Shi, J., Zhao, Y., Wang, K., Shi, X., Wang, Y., Huang, H., Zhuang, Y., Cai, T., Wang, F., and Shao, F.** (2015). Cleavage of GSDMD by inflammatory caspases determines pyroptotic cell death. *Nature* **526**, 660-665.
- Silveira, F.T., Lainson, R., and Corbett, C.E.** (2004). Clinical and immunopathological spectrum of American cutaneous leishmaniasis with special reference to the disease in Amazonian Brazil: a review. *Memorias do Instituto Oswaldo Cruz* **99**, 239-251.
- Swanson, K.V., Deng, M., and Ting, J.P.** (2019). The NLRP3 inflammasome: molecular activation and regulation to therapeutics. *Nature reviews Immunology* **19**, 477-489.
- Takenouchi, T., Nakai, M., Iwamaru, Y., Sugama, S., Tsukimoto, M., Fujita, M., Wei, J., Sekigawa, A., Sato, M., Kojima, S., et al.** (2009). The activation of P2X7 receptor impairs lysosomal functions and stimulates the release of autophagolysosomes in microglial cells. *Journal of immunology* **182**, 2051-2062.
- Zamboni, D.S., and Sacks, D.L.** (2019). Inflammasomes and *Leishmania*: in good times or bad, in sickness or in health. *Current opinion in microbiology* **52**, 70-76.



## Figures



**FIGURE 1: Description of assay and readouts to monitor *L. amazonensis*-infected BMDMs undergoing pyroptosis.**

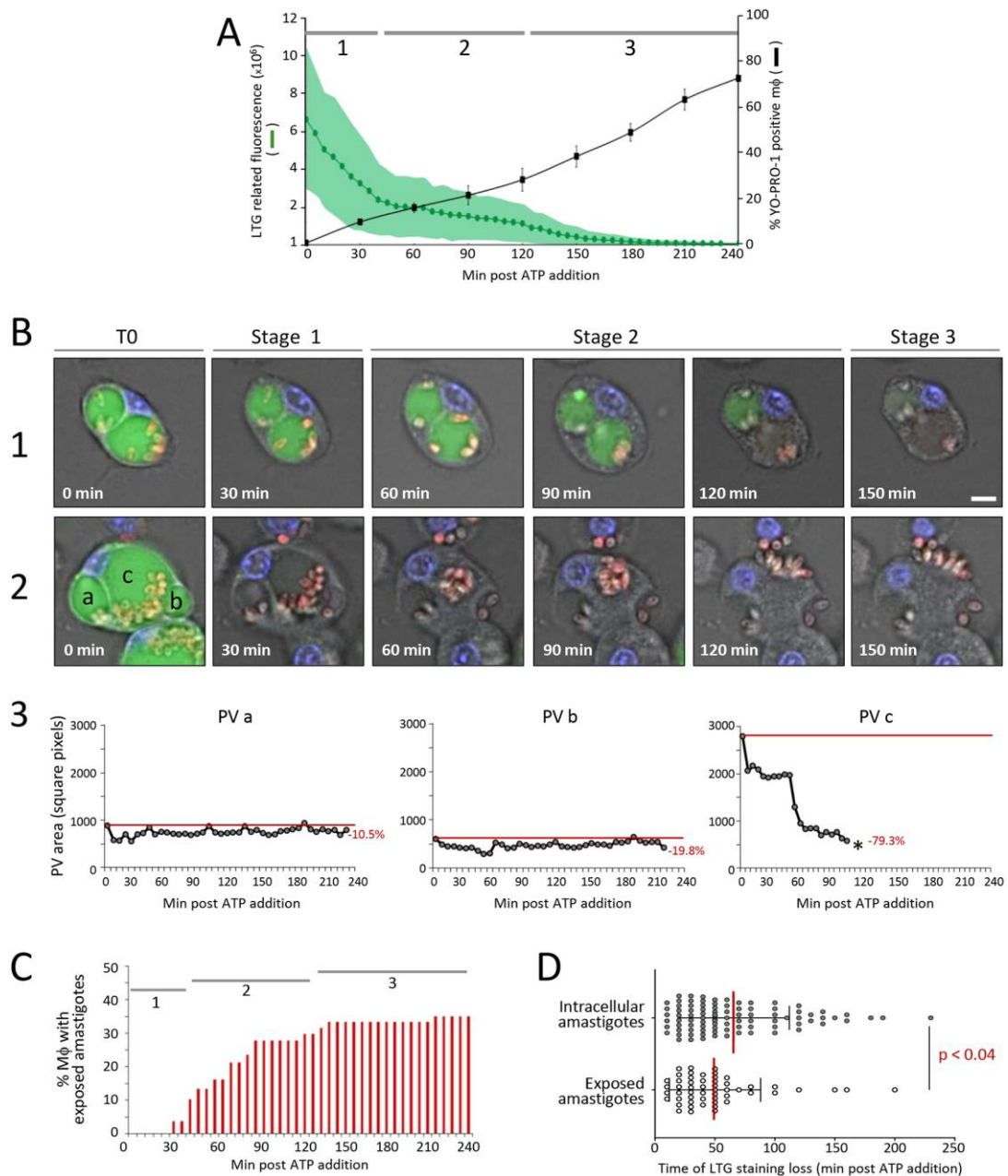
**(A) Experimental flow chart.** Mouse BMDMs were differentiated from bone marrow progenitors in the presence of mCSF1 and seeded in 96-well plates. Five hours later, mCherry lesion-derived amastigotes of *L. amazonensis* (*L. am*) were added to BMDMs (MOI = 4:1, 72 hours, 34°C). NLRP3 was primed adding 500 ng/ml LPS for 3h45 min. Then fluorescent reporters Hoechst 33342 (Ho 33342), LysoTracker Green DND-26 (LTG) and YO-PRO-1 were added. Finally, pyroptosis was triggered by NLRP3 activation with 5 mM ATP. Real-time analyses were performed using the OPERA™ plate reader at 34°C, 7.5% CO<sub>2</sub> for 240 min.

**(B) High Content Assay read-outs.** Image acquisition was performed every 5 min. A representative field image is displayed for each channel (T0 time point for Ho 33342, LTG, mCherry and Transmitted Light (TL); T = 120 min for YO-PRO-1 staining). Macrophage nuclei were stained by Ho 33342 (blue channel, panel B1). Nuclei of pyroptotic macrophages were stained by YO-PRO-1 (green channel, panel B2). PV integrity and acidity were evaluated by the LTG staining (green channel, panel B3). Parasite location was determined by the mCherry fluorescence signal (red channel, panel B4) in relation to the macrophage body (TL, panel B5). Macrophage area was evaluated on TL pictures. Scale bar = 20 μm.



**(C) HCA analysis quality controls.** HCA analyses were performed at the population level analyzing 15 000 cells per well. Three quality controls were performed by: i) monitoring macrophage numbers to control that no cells were lost during the analysis (C1), ii) analyzing the percentage of dead macrophages (YO-PRO-1 positive) 4 hours post ATP addition to control for efficient pyroptosis induction (C2, at least 70% of death must be observed at this time point), and iii) assessing LTG fluorescence at T0 and T240 to monitor PV presence (T0) and pyroptosis associated with the complete loss of PV staining (T240, C3).

**(D) Single cell analyses.** Merged pictures (Ho 33342, LTG, mCherry and TL images) of representative infected macrophages (T0). Identification and quantification of areas of PVs (a), (b) and (c) and parasite location. The unit of PV area is square pixels.



**FIGURE 2: Real-time multiparametric analysis of pyroptotic *L. amazonensis*-infected macrophages.**

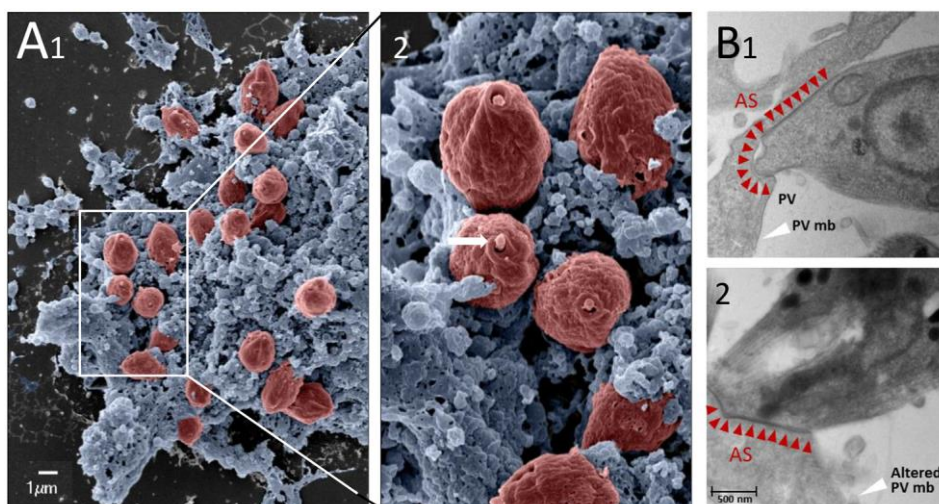
Pyroptosis was induced in *L. amazonensis*-infected BMDMs by LPS and ATP. Real-time analyzes were performed to follow macrophage pyroptosis and amastigote localization during 240 minutes.

**(A) High Content Assay analysis of PV acidity and macrophage mortality.** Macrophage pyroptosis (mean YO-PRO-1 positive macrophages  $\pm$  SEM, black curve) and PV acidity (mean LTG fluorescence  $\pm$  SEM, green curve and green area, respectively,  $n=2$  independent

experiments) were monitored. Three stages were delineated according to the decay rate of LTG fluorescence.

**(B) Real-time, single cell monitoring of infected macrophages.** Merged images for Ho 33342, LTG, mCherry fluorescence and TL acquired from two representative macrophages during the first 150 min. Acquisition was performed before ATP addition (T0) and during the pyroptosis stages defined in Fig. 2A1. (B1) Macrophage displaying two PVs with different LTG decay rates and maintaining amastigotes intracellularly. Scale bar = 10  $\mu$ m. (B2) Macrophage displaying 3 PVs (a, b, c), with one cell exposing amastigotes to the extracellular milieu (c). (B3) Area of PVs (a), (b) and (c) of the macrophage displayed in B2. The red line corresponds to the initial value of the corresponding PV area. The number corresponds to the % of reduction of PV area at the final time point versus the initial value (T0).

**(C) Single cell monitoring of surface amastigote exposition.** The percentage of macrophages exposing amastigotes at their surface was determined every 30 min (single cell analysis, n= 384 macrophages). The three pyroptosis stages are indicated. (D) Relationship between amastigote location and LTG staining decay. The time point at which LTG staining is lost is indicated for macrophages with intracellularly retained (black dots) or surface exposed (white dots) amastigotes. The statistical significance between the two groups is indicated (p value).

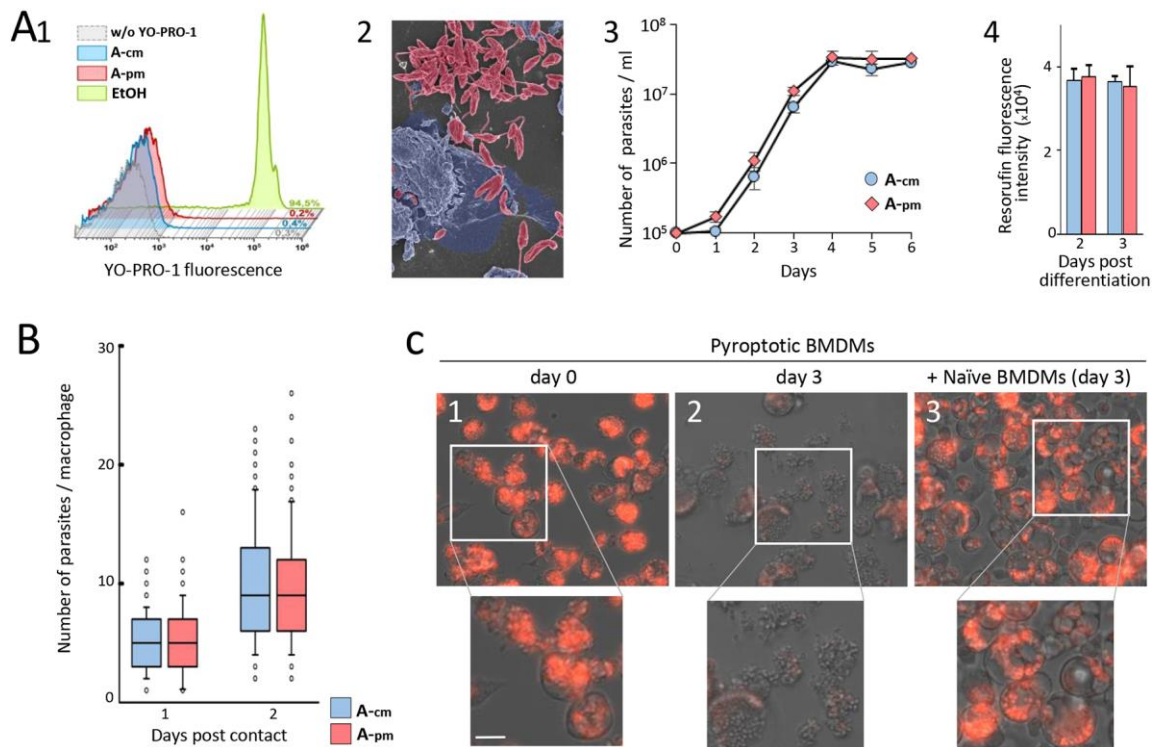


**FIGURE 3: Amastigotes are exposed during macrophage pyroptosis.**

Pyroptosis was induced in *L. amazonensis*-infected BMDMs by LPS and ATP stimulation.

**(A) Scanning electron microscopy analysis of a representative pyroptotic macrophage exposing amastigotes (pseudo-colored in red) at the cell surface (1).** Zoomed picture (2) highlights the orientation of attached parasites with the flagellar pocket pointing towards the extracellular milieu (white arrow).

**(B) TEM images showing the Attachment Site (AS, red arrowheads) of an amastigote in untreated (1) and pyroptotic (2) macrophages.** Note the unaltered PV membrane at the AS in the pyroptotic macrophage that contrasts with altered nearby membranes. White arrowheads point to the PV membrane. "PV" indicates the PV lumen.



**FIGURE 4: Amastigotes derived from pyroptotic macrophages are viable and virulent.** Parasites isolated from pyroptotic (A-pm) and control unstimulated (A-cm) macrophages were compared.

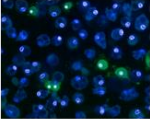

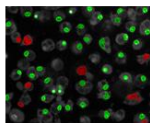
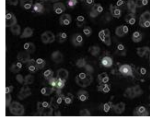
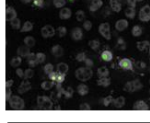
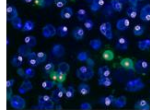
**(A) Assessment of viability and amastigote-to-promastigote differentiation capacity.** (1) FACS analysis of YO-PRO-1 incorporation of isolated amastigotes and ethanol-killed parasites (positive control for cell death). Percentages of YO-PRO-1<sup>+</sup> parasites are indicated. (2) Scanning electron microscopy pseudo-colored image of a representative pyroptotic macrophage 4 hours after pyroptosis induction and maintained in promastigote medium (27°C, 48 hours). Promastigotes were pseudo-colored in red. (3) Growth curves for A-pm and A-cm (27°C). (4) Assessment of metabolic activity of A-pm- and A-cm-derived promastigotes (raw resorufin fluorescence values are shown).

**(B) Evaluation of amastigote virulence.** A-pm and A-cm were added to cultures of naïve BMDMs for one and two days. Parasite number per macrophage is shown (n = 2 independent experiments). (C) Evaluation of the capacity of amastigotes attached to pyroptotic remnants to infect naïve macrophages. Naïve BMDMs were added to pyroptotic *L. amazonensis*-infected macrophages in fresh medium (34°C, 3 days) and analyzed by epifluorescence and phase contrast microscopy. Representative fields and a cropped zoomed area are shown (upper and

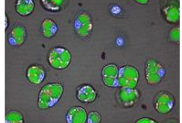
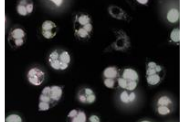
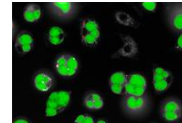
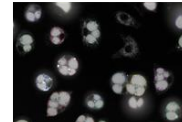
lower panels, respectively). Scale bar: 20  $\mu\text{m}$ . Pyroptotic macrophages at day 0 (1) and 3 (2). The loss of mCherry fluorescence was probably due to parasite death in absence of host cells. (3) Pyroptotic macrophages at day 3 post addition of naïve macrophages (Representative pictures, n = 2 independent experiments).



**A**

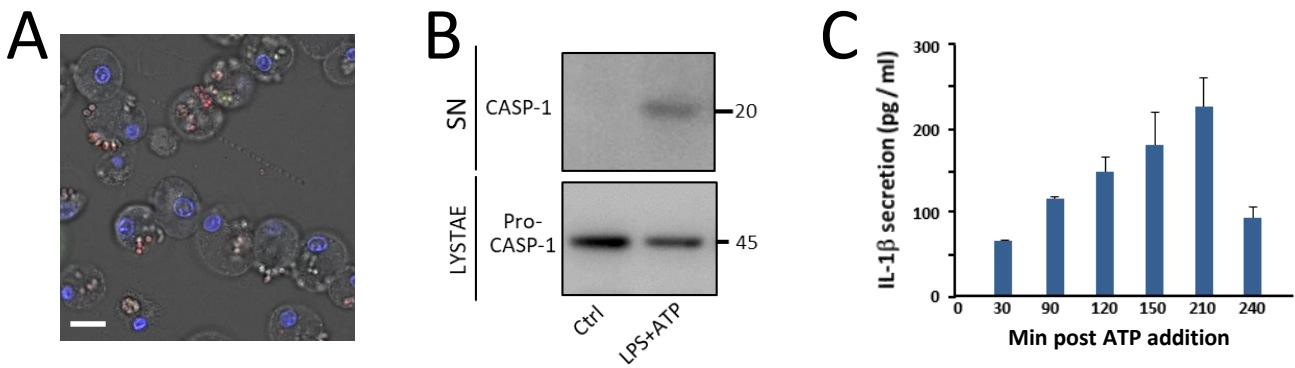
<b>1. Input Image</b>		Stack Processing: Individual Planes Flatfield Correction: None	
			
<b>2. Signal segmentation – Hoechst 33342</b>		Channel: Exp1Cam1 ROI: None	Method: A Common Threshold: <u>0.35</u> Area: > <u>1</u> $\mu\text{m}^2$ Split Factor: 68 Individual Threshold: <u>0.2</u> Contrast: > <u>0.45</u>
			Output Population: Nuclei
	a) Calculate Intensity Properties	Channel: Exp1Cam1 Population: Nuclei Region: Nucleus	Method: Standard Mean Output Properties: Intensity Nucleus Exp1Cam1
	b) Calculate Morphology Properties	Population: Nuclei Region: Nucleus	Method: Standard Area Roundness Output Properties: Nucleus
<b>3. Population selection – Hoechst 33342</b>		Population: Nuclei	Method: Filter by Property Nucleus Roundness: > <u>0.6</u> Intensity Nucleus Exp1Cam1 Mean: > <u>500</u> Boolean Operations: F1 and F2
			Output Population: Nuclei Selected
<b>4. Signal segmentation – YO-PRO-1</b>		Channel: Exp2Cam1 ROI: Nuclei Selected ROI Region: Nucleus	Method: M Diameter: <u>2</u> $\mu\text{m}$ Splitting Coefficient: <u>0.1</u> Common Threshold: <u>0.4</u>
			Output Population: YO-PRO-1 Nuclei
	a) Calculate Intensity Properties	Channel: Exp2Cam1 Population: YO-PRO-1 Nuclei Region: Nucleus	Method: Standard Mean Output Properties: Intensity Nucleus Exp2Cam1
<b>5. Population selection – YO-PRO-1</b>		Population: YO-PRO-1 Nuclei	Method: Filter by Property Intensity Nucleus Exp1Cam1 Mean: > <u>250</u>
			Output Population: YO-PRO-1 Nuclei Selected
<b>6. Define results</b>		Method: List of Outputs Population: Nuclei Selected Number of Objects: Apply to All:	
		Population: YO-PRO-1 Nuclei Selected Number of Objects: Apply to All	
		Population: Nuclei Selected: ALL YO-PRO-1 Nuclei Selected: ALL	

**B**

<b>1. Input Image</b>		Stack Processing: Individual Planes Flatfield Correction: None	
			
<b>2. Signal segmentation</b>		Channel: Exp2Cam1 ROI: None	Method: M Diameter: <u>5</u> $\mu\text{m}$ Splitting Coefficient: <u>0</u> Common Threshold: <u>0.3</u>
			Output Population: Lyso
	a) Calculate Intensity Properties	Channel: Exp2Cam1 Population: Lyso Region: Cell	Method: Standard Mean Sum Output Properties: Intensity Cell Exp2Cam1
	b) Calculate Morphology Properties	Population: Lyso Region: Cell	Method: Standard Area, Roundness Output Properties: Cell
<b>3. Population selection</b>		Population: Lyso	Method: Filter by Property Cell Area [ $\mu\text{m}^2$ ]: > <u>5</u> Cell Roundness: > <u>0.45</u> Boolean Operations: F1 and F2
			Output Population: Lyso Selected
<b>4. Define results</b>		Method: List of Outputs Population: Lyso Selected Number of Objects Apply to All Intensity Cell Exp2Cam1 Mean Intensity Cell Exp2Cam1 Sum Cell Area [ $\mu\text{m}^2$ ], Cell Roundness	
		Population: Lyso Selected: ALL	

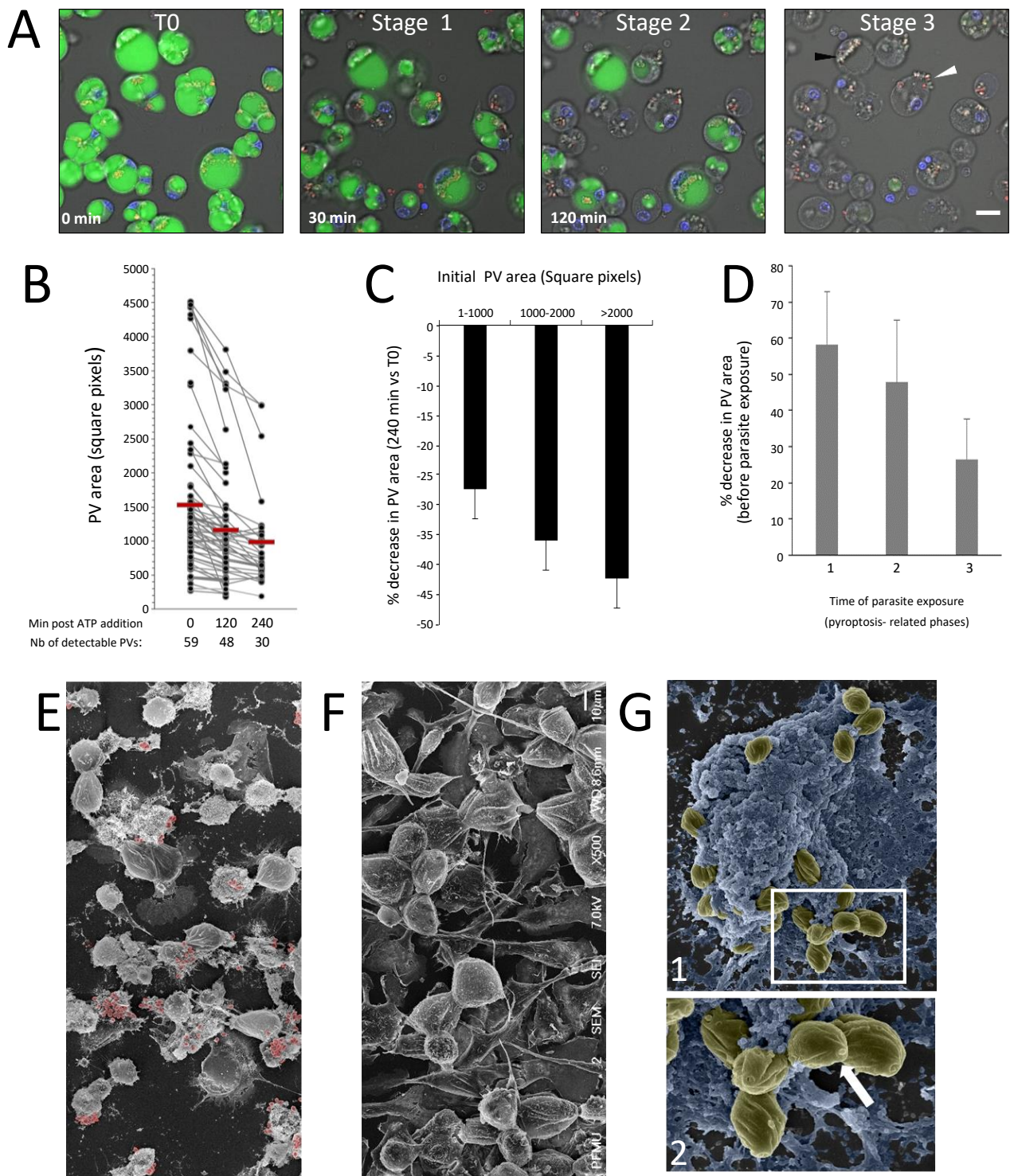
**FIGURE S1: Automatic image analysis procedure to monitor macrophage pyroptosis in *L. amazonensis*-infected BMDMs.**

Live imaging was performed with the OPERA™ plate reader every 5 minutes following pyroptosis induction (ATP addition). Images were transferred to the Columbus Conductor™ Database and analyzed using the integrated Image analysis building blocks. (A) The sequential image segmentation process showing the identification and counting of Hoechst 33342-stained living/dead macrophages are shown for YO-PRO-1-stained dying cells. (B) The sequential image segmentation process showing the identification and counting of Hoechst-stained living/dead macrophages are shown for LTG-stained PVs.



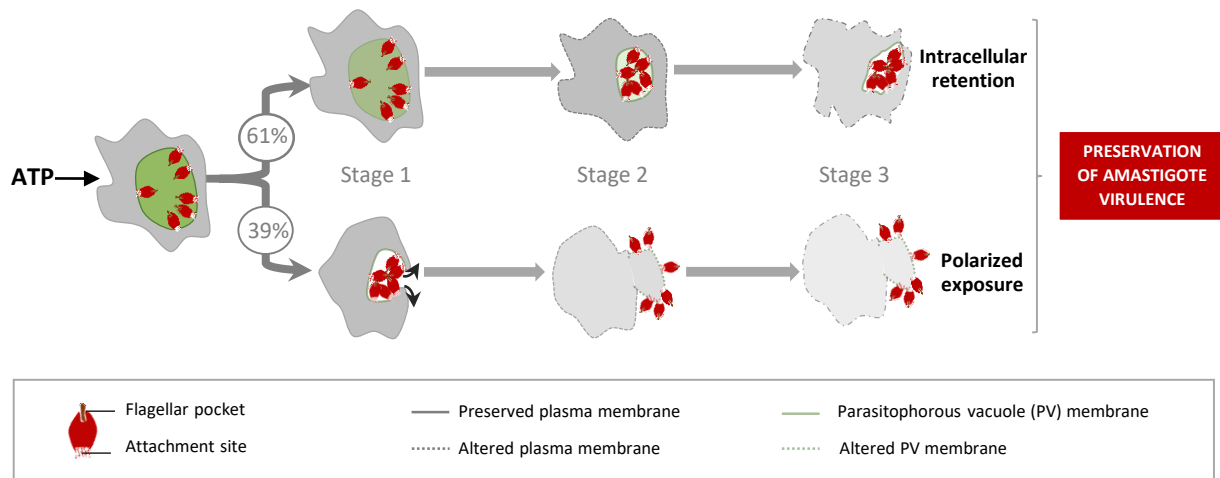
**FIGURE S2: LPS/ATP-treated *L. amazonensis*-infected macrophages die by pyroptosis** (A) Representative image of *L. amazonensis* infected BMDMs after LPS stimulation and 4 hours of ATP stimulation obtained with the OPERA™ plate reader. A merge of the Hoechst 33342, mCherry, and bright field images is shown. The round swollen shape of both the cell body and the nucleus are typical for pyroptotic cells. Scale bar: 20 μm. (B) Detection of the release of cleaved caspase-1 in the supernatant (SN) from LPS and ATP-treated versus unstimulated (ctrl) infected BMDMs by Western blotting. Detection was performed 4 hours post ATP addition. (C) Evidence for IL-1 secretion following ATP addition as detected by ELISA.





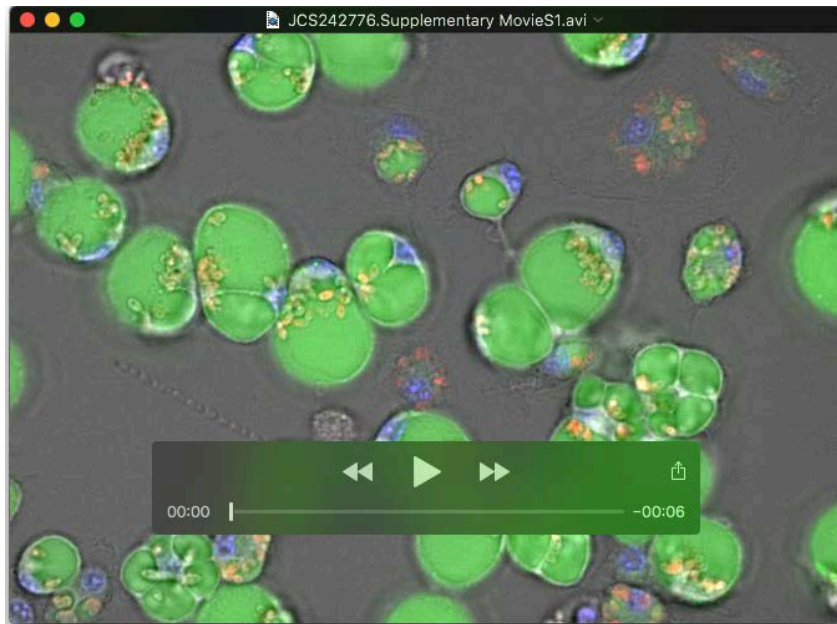
**FIGURE S3: Characteristics of PVs and amastigotes during macrophage pyroptosis.**

(A) representative field of infected macrophages at 3 time points corresponding to the 3 pyroptotic-related stages. The merged fluorescence and bright field images illustrate the behavior of LTG-stained PVs and mCherry-expressing amastigotes in Hoechst 33342-stained macrophages. Note the different location of amastigotes, either within PV (black arrow) or exposed to the outside milieu (white arrow) 240 min after ATP addition. Scale bar: 20  $\mu$ m. (B) Monitoring of Individual PV area at 3 time points. Note the disappearance of some PVs at 240 min. (C) Relationship between the initial PV size and the extent of area reduction. The % of area reduction was recorded at 240 min for every single PV and classified in 3 categories depending on their initial size at 0 min. (D) Relationship between PV area reduction and parasite exposure for the 3 stages. (E-G) Scanning Electron Microscopy was performed on *L. amazonensis* (E, F) and *L. donovani* (G)-infected BMDMs. (E) Representative image of pyroptotic macrophages after 3 hours of ATP stimulation. Amastigotes are attached to dead macrophages and exposed to the extracellular milieu (red colorization). (F) Representative image of an untreated macrophages. Big globular cells correspond to heavily infected macrophages harboring large PVs. (G) Image of a representative pyroptotic *L. donovani*-infected BMDM. The exposition at the cell surface of *L. donovani* amastigotes (olive colorization, 1) is similar to that of *L. amazonensis* parasites and reveals the parasite flagellar pocket pointing towards the extracellular milieu (arrow, zoomed area, 2).



**FIGURE S4: Schematic overview recapitulating the fate of intracellular *Leishmania* during macrophage pyroptosis.**

The induction of pyroptosis in *Leishmania*-infected macrophages by ATP leads to two different scenarios. In both cases, PVs decay with a loss of LTG fluorescence, with or without reduction in area: In 61% of macrophages, a slow reduction of LTG staining occurs, with PV maintained *in cellula* and intracellular retention of virulent amastigotes (upper part). In 39% of macrophages, PVs decay faster and the inner part of the PV membrane is exposed on the macrophage surface (Exposure of the Luminal side of the parasitophorous Vacuole, ELV). ELV leads to the polarized exposure of virulent amastigotes that are maintained embedded in PV membranes (lower part). Parasite exposure occurs only during the first two stages of pyroptosis. The third stage is associated to more pronounced cellular alterations.



**Movie 1: Real-time multiparametric analysis of *L. amazonensis*-infected macrophages during pyroptosis.**

Pyroptosis was induced in *L. amazonensis*-infected BMDMs by sequential stimulation with LPS and ATP. Real-time analyzes were performed to follow macrophage pyroptosis and amastigote localization during 240 minutes after ATP addition using the OPERA™ plate reader at 34°C, 7.5% CO<sub>2</sub>. The movie was realized with sequential analyses of merged images for Ho 33342, LTG, mCherry fluorescence and TL pictures taken every 5 minutes.